

# Carbon Dots with Continuously Tunable Full-Color Emission and Their Application in Ratiometric pH Sensing

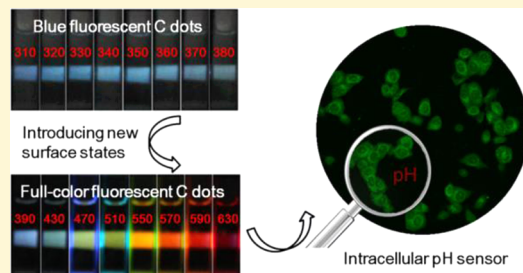
Hui Nie,<sup>†</sup> Minjie Li,<sup>\*,†</sup> Quanshun Li,<sup>‡</sup> Shaojun Liang,<sup>‡</sup> Yingying Tan,<sup>‡</sup> Lan Sheng,<sup>†</sup> Wei Shi,<sup>‡</sup> and Sean Xiao-An Zhang<sup>\*,†</sup>

<sup>†</sup>State Key Laboratory of Supramolecular Structure and Materials, College of Chemistry, Jilin University, Changchun 130012, P.R. China

<sup>‡</sup>Key Laboratory for Molecular Enzymology and Engineering of the Ministry of Education, College of Life Science, Jilin University, Changchun 130012, P.R. China

## Supporting Information

**ABSTRACT:** Two types of carbon dots (C dots) exhibiting respective excitation-independent blue emission and excitation-dependent full-color emissions have been synthesized via a mild one-pot process from chloroform and diethylamine. This new bottom-up synthetic strategy leads to highly stable crystalline C dots with tunable surface functionalities in high reproducibility. By detailed characterization and comparison of the two types of C dots, it is proved concretely that the surface functional groups, such as C=O and C=N, can efficiently introduce new energy levels for electron transitions and result in the continuously adjustable full-color emissions. A simplified energy level and electron transition diagram has been proposed to help understand how surface functional groups affect the emission properties. By taking advantage of the unique excitation-dependent full-color emissions, various new applications can be anticipated. Here, as an example, a ratiometric pH sensor using two emission wavelengths of the C dots as independent references has been constructed to improve the reliability and accuracy, and the pH sensor is applied to the measurement of intracellular pH values and cancer diagnosis.



## ■ INTRODUCTION

Carbon dots (C dots) represent an important class of photoluminescent (PL) nanomaterials due to their attractive properties, including less toxicity, good compatibility, and relatively easy surface modification, etc.<sup>1–3</sup> Until now, C dots have been prepared by a variety of approaches ranging from top-down to bottom-up strategies<sup>4–10</sup> and have been applied widely in fields of bioimaging,<sup>3,11–15</sup> printing inks,<sup>16</sup> photocatalysis,<sup>17,18</sup> and sensors.<sup>19–22</sup> Among these works, one of the most studied properties is the excitation-dependent vs the excitation-independent features of emission for C dots.<sup>23</sup> However, understanding and engineering the unique excitation-dependent emission is very hard, and most of the known C dots have emissions centered in the blue and green regions without using color filters, which is not preferred for biological applications because of the harm of their short wavelength excitation light to living cells or biosystems.<sup>24</sup> It is ideal that the C dots can exhibit continuously adjustable excitation-dependent full-color emission with comparable intensities, because it will realize any visible color by selecting different excitation wavelengths without changing the chemical structure. And this will enable the C dots to integrate with a wide range of photoluminescent objects and construct multifunctional sensing systems without considering the match of energy gaps. Therefore, it is of great importance to explore C dots with intrinsic full-color emission.

To achieve the above-mentioned aim, it is primary to truly understand the factors that affect the emission properties of C dots. Very similar to the well-developed II–VI and III–V semiconductor quantum dots (QDs), several factors, such as the size (or the size distribution),<sup>8</sup> element doping,<sup>23,25</sup> and the surface states<sup>26</sup> of C dots, have been reported so far that influence their emission properties greatly. Especially are the relative abundant surface groups found to directly relate to the emission intensity and band shape.<sup>26</sup> However, the way by which these surface groups affect their emission is still poorly understood, and further study on tuning the emission of C dots by the engineering of surface states has seldom been done. Therefore, it is of particular significance to obtain deep insight into the mechanism of the surface chemistry of C dots and to further develop applicable strategies for engineering their emission behaviors rationally.

Herein, we present a new strategy of selectively preparing two types of C dots with either excitation-independent blue emission or distinctive excitation-dependent full-color emissions from chloroform ( $\text{CHCl}_3$ ) and diethylamine (DEA) by varying the reaction conditions. This method is highly reproducible, and the obtained C dots are fairly stable and compatible with a variety of solvents. The two types of the as-

Received: January 29, 2014

Revised: April 18, 2014

Published: April 22, 2014



synthesized C dots supply ideal objects for investigating the origin of the full-color emissions. By detailed characterization and comparison of the two types of C dots, it is proved concretely that the surface functional groups, such as C=O and C=N, can efficiently introduce new energy levels for electron transitions and result in the continuously adjustable excitation-dependent full-color emissions with comparable intensities. Taking advantage of their unique emission properties, the C dots were applied as an internal reference to construct a ratiometric pH sensor.

## RESULTS AND DISCUSSION

### Preparation and Characterization of Blue Fluorescent C Dots (B-C dots) and Full-Color Fluorescent C Dots (F-C dots).

C dots have been reported to be prepared from an abundance of resources, such as resols, carbohydrates, citrate acid, and others.<sup>4–7</sup> Here, by refluxing CHCl<sub>3</sub> and DEA for different times, C dots with distinct fluorescent properties can be obtained (Figure 1a). First, B-C dots were synthesized by

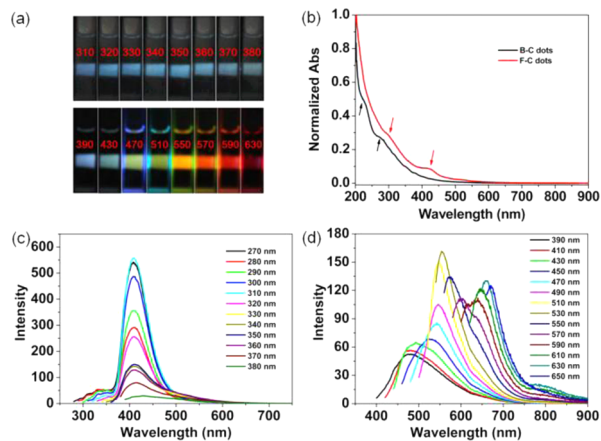


**Figure 1.** (a) Fluorescence images of B-C dots (upper row) and F-C dots (lower row) in ethanol excited with the indicated wavelengths; (b) UV-visible absorption spectra of the B-C dots and F-C dots in ethanol; (c, d) Fluorescence spectra of the B-C dots (0.025 mg/mL) and F-C dots (0.02 mg/mL) in ethanol under different excitation wavelengths.

refluxing the reactants for 1 h and then purifying by dialysis to remove the small residues. When the reaction time was prolonged to 60 h, another fraction of C dots with amazing excitation-dependent full-color emission (F-C dots) were also obtained. Because the polarities of these two fractions are quite different, they can be further separated simply by column chromatography. The optical properties of the B-C dots and F-C dots in ethanol are shown in parts b–d of Figure 1. In the UV-vis spectra, the B-C dots exhibit two shoulder absorption peaks at 228 and 282 nm, which have been observed in a wide range of C dots prepared by other methods.<sup>27,28</sup> Differently, F-C dots exhibit two shoulder absorption peaks at 300 and 421 nm. The different types of electron transition corresponding to these absorption peaks will be investigated in detail in the next section. In the fluorescence spectra, B-C dots show an excitation-independent emission peak at 407 nm with bandwidth of ~61 nm (Figure 1c). In addition, the fluorescence spectra feature small tails extending into the long wavelength region. However, the F-C dots show nearly continuous excitation-dependent emission without additional surface

passivation. It is worth noting that F-C dots have selective emission in a broad color range over the entire visible region, with the emission peak wavelengths ranging from 470 nm (blue) to 670 nm (red) with the excitation from 390 to 650 nm (Figure 1d). The detailed emission properties of F-C dots including emission wavelengths ( $\lambda_{em}$ ) at different excitation wavelengths ( $\lambda_{ex}$ ),  $\Delta\lambda$  ( $\lambda_{em} - \lambda_{ex}$ ), emission intensity, and bandwidth are illustrated in Table S1 in the Supporting Information (SI). The change of emission intensities and  $\Delta\lambda$  with emission positions is not regular; meanwhile, all the emission band shapes are asymmetric with small tails extending to long wavelength. These phenomena suggest the PL of F-C dots are related not only with the size distribution but also with the diversified surface states.<sup>8</sup>

The diameters of the B-C dots and F-C dots are centered at 1–3 nm and 2–4 nm, respectively, from transmission electron microscopy (TEM) images (Figure 2). High-resolution TEM

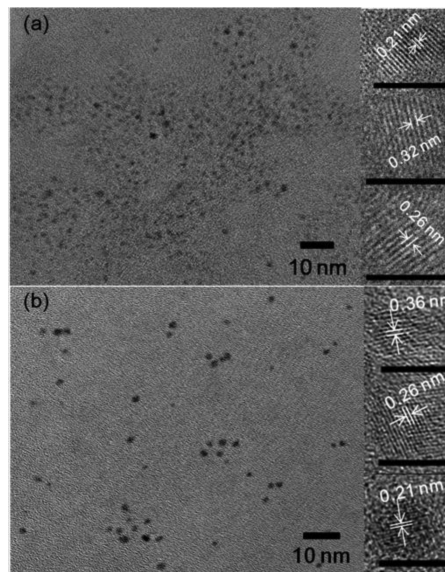


**Figure 2.** TEM and HRTEM images of the B-C dots (a) and F-C dots (b). Scale bar = 5 nm in HRTEM images.

(HRTEM) images of B-C dots show well-resolved lattice fringes with interplanar spacings of 0.21, 0.26, and 0.32 nm which are close to the (100), (020) and (002) diffraction facets of graphite carbon, respectively.<sup>29</sup> Similar crystallinity with lattices of 0.21, 0.26, and 0.36 nm are also found in F-C dots. The Raman peaks centered at  $\sim$ 1360 and 1590 cm<sup>-1</sup> for the two C dots are attributed to the D and G bands of carbon materials representing the sp<sup>3</sup> and sp<sup>2</sup> carbon, respectively (Figure S1 in the SI).<sup>30</sup> Thus, the above results suggest that both B-C dots and F-C dots are composed of nanocrystalline cores of graphitic sp<sup>2</sup> carbon atoms and that there are sp<sup>3</sup> carbon defects in the cores or on the surfaces.

The chemical compositions and structures of the B-C dots and F-C dots are further investigated. X-ray photoelectron spectroscopy (XPS) survey spectra show that carbon (C 1s, 284 eV), nitrogen (N 1s, 399 eV), and oxygen (O 1s, 532 eV) elements were contained in both of the B-C dots and F-C dots. Meanwhile, trace quantities of chlorine (Cl) with their Cl 2p and Cl 2s peaks at 197 and 267 eV are also observed (Figure 3a).<sup>31</sup> Even though no oxygen-containing starting materials were used in this reaction, the O signal is observed. As our reaction was carried out under air by heating, oxygen in the air

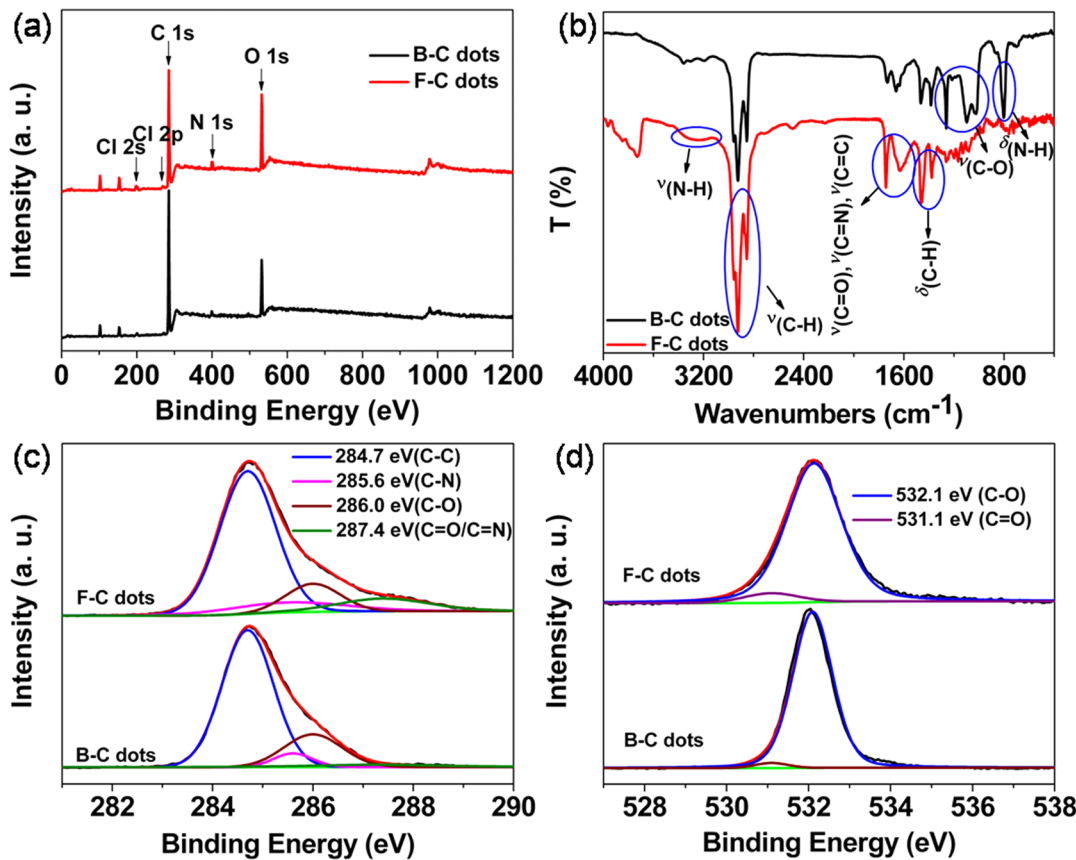


**Figure 3.** (a) XPS patterns of the B-C dots and F-C dots; (b) FT-IR spectra of B-C dots and F-C dots; (c, d) High-resolution XPS spectra of the C 1s and O 1s peaks of B-C dots and F-C dots, respectively.

can be introduced into this system easily through an oxidation reaction.<sup>32</sup> The detailed formation mechanism of our C dots will be explained later. Elemental analysis also confirms the composition of these two kinds of C dots (B-C dots: C 72.42 wt %, H 12.64 wt %, N 2.4 wt %; F-C dots: C 60.12 wt %, H 9.02 wt %, and N 5.62 wt %).

In the Fourier transform infrared spectroscopy (FT-IR) analysis of B-C dots and F-C dots, the absorption bands at 3328 and 3217  $\text{cm}^{-1}$  corresponding to stretching vibration of N–H, stretching and bending vibrations of  $\text{CH}_3$  and  $\text{CH}_2$  at around 2975, 2927, 2854  $\text{cm}^{-1}$  and 1460, 1380  $\text{cm}^{-1}$  are observed in both C dots (Figure 3b). In addition, they exhibit the characteristic absorption bands of C=C at 1641  $\text{cm}^{-1}$ .<sup>33</sup> However, compared with B-C dots, the intensity of C–O vibrations at 1250  $\text{cm}^{-1}$ , the asymmetric and symmetric stretching vibrations of C–O–C at 1095 and 1020  $\text{cm}^{-1}$ , and the N–H deformation vibration at 800  $\text{cm}^{-1}$  are reduced distinctly for F-C dots, accompanied by increased intensity of C=O and C=N stretching vibrations at 1749 and 1668  $\text{cm}^{-1}$ , respectively.<sup>27,34</sup> More information on differences in surface functional groups of the B-C dots and F-C dots is further provided by XPS analysis (parts c and d of Figure 3). The high-resolution C 1s spectra reveal the presence of C=C (284.7 eV), C–N (285.6 eV), C–O (286.0 eV), and C=N/C=O (287.4 eV). The relative contents of the different chemical states of these two C dots are calculated on the basis of their integral area as shown in Table S2 in the SI. The content of C=O/C=N for F-C dots is ~9.2%, higher than that of B-C dots (~4.3%). And the content of C–O in F-C dots is 13.7%, which is lower than that of B-C dots (19.1%). Consistent with

the analysis of C 1s spectra, N 1s spectra also confirm that the N content of F-C dots is higher than that of B-C dots, and the N/C ratios of B-C dots and F-C dots are 0.011:1 and 0.052:1, respectively. High-resolution N 1s spectra reveal that N exists in the forms of C–N (399.3 eV) and C=N (401.6 eV) for F-C dots<sup>35</sup> and in the form of C–N (399.3 eV) for B-C dots (Figure S2 in the SI). The O 1s spectra of these two C dots exhibit two peaks at 531.1 and 532.1 eV, which are attributed to C=O and C–OH/C–O–C groups, respectively. Meanwhile, the percentage of C=O in F-C dots is higher than that in B-C dots. These results from XPS data are in good accordance with FT-IR analysis. From the above data, it is clear that the composition and functional groups on the surface of the two C dots alter a lot, and the F-C dots have more oxygen and nitrogen percentages in the forms of C=O/C=N than B-C dots. Presumably, various structural configurations with those functional groups result randomly during the process of F-C dots generation, and this will lead to diversified surface states.

Due to the small size and multitudinous functional groups on the surface of C dots, the C dots have high compatibility and are miscible in various solvents, such as water, ethanol, ethyl acetate, dimethylformamide, dimethyl sulfoxide,  $\text{CH}_2\text{Cl}_2$ , etc.<sup>11</sup> Then detailed studies designed to describe the fluorescent properties of the F-C dots are carried out. Parts a and b of Figure S3 in the SI show the intensity variation at two emission positions (555 and 660 nm) of F-C dots with concentration. When the concentration of F-C dots solutions is lower than 0.08 mg/mL, the fluorescence intensity decreases linearly with concentration and the intensity ratio of 555 nm ( $\lambda_{\text{ex}} = 530 \text{ nm}$ ) to 660 nm ( $\lambda_{\text{ex}} = 630 \text{ nm}$ ) remains unchanged. The data show

that the full-color emission of F-C dots derives from a single particle rather than combination of multiple C dots with different emission wavelengths.

Compared with other full-color emission systems, such as organic compounds with multiple chromophores and GaN quantum dots etc.,<sup>36–38</sup> our C dots have the advantages of easy preparation under very mild reaction conditions and very low toxicity with the attractive characteristics of continuous excitation-dependent full-color emission. The PL properties of B-C dots and F-C dots in water and ethanol were compared in detail (Figure S4 in the SI). It was found that the PL intensity of both B-C dots and F-C dots decreased from ethanol to water. However, the emission positions of B-C dots were more sensitive to solvent polarity than those of F-C dots, which may be attributed to their relatively smaller size. To our delight, the excitation-independent or excitation-dependent PL properties of these two C dots remained almost unchanged, suggesting that their unique PL properties can be exploited for various applications in these solvent systems. In addition, the preparation was highly reproducible, which was proved definitely by approximately the same fluorescence spectra (with a deviation of  $\pm 2.5\%$  from the average) of the C dots from three parallel batches under the same reaction conditions as shown in Figure S5 in the SI. Moreover, the C dots showed considerable stability with no attenuation in fluorescence intensity after storage for 3 months under ambient conditions (Figure S6 in the SI).

Then the PL stability of these two C dots to the effect of pH (0–13) was investigated. Emission intensities of both the B-C dots and F-C dots changed slightly from pH 3 to 10, while they decreased significantly in lower or higher pH conditions (Figure S7 in the SI). The effect of temperature on the PL properties of B-C dots and F-C dots was investigated in aqueous solution from 278 to 348 K. The PL intensity of B-C dots first decreased over the temperature range of 278 to 298 K, and then almost remained unchanged with elevated temperature. For the F-C dots, The emission intensities at various emission positions all showed monotonous decreases with temperature, and the Arrhenius plots for these peaks revealed that the fluorescence intensities in the green and red regions decreased much faster than intensities in the blue region as shown in Figure S8 in the SI, suggesting that the emissions in the blue region and the green to red region may originate from different electron transitions. This temperature-induced PL quenching was suggested to be highly related to the enhanced nonradiative relaxation.<sup>39,40</sup> The quantum yield (QY) of the resulting B-C dots and F-C dots in ethanol were 17.1% and 12.6% (using anthracene and rhodamine B as references with excitation wavelengths of 350 and 550 nm, respectively). Then the approximate QY of F-C dots at other wavelengths were calculated using itself (QY measured with excitation wavelength of 550 nm) as reference (Figure S9 in the SI).

#### Origin of the Full-Color Fluorescence of the F-C Dots.

Here, B-C dots and F-C dots with distinct emission properties were synthesized by simply tuning the reaction time via the same one-pot synthesis process. So what are the key factors that contribute to their emission properties? Previous reports have pointed out that quantum effect, surface states, and zigzag sites can greatly affect the emission properties of C dots.<sup>8,26,41</sup> Here, we try to correlate their structures with their emission properties, just as we conclude above that F-C dots and B-C dots differ a lot in percentage of oxygen and nitrogen in the forms of C=O/C=N. We conjecture that the full-color

emission of the F-C dots is highly related to the C=O and C=N functional groups on their surface, which can generate abundant structural configurations and introduce new energy levels into their electronic structures, and consequently result in more electronic transition possibilities. In order to clarify this deduction, the C=O and C=N functional groups on the surface of F-C dots are selectively reduced by NaBH<sub>4</sub>.<sup>26,42,43</sup> The reduction process can be confirmed by FT-IR analysis. As shown in Figure 4a, the absorption of O-H (3446 cm<sup>-1</sup>), C-O

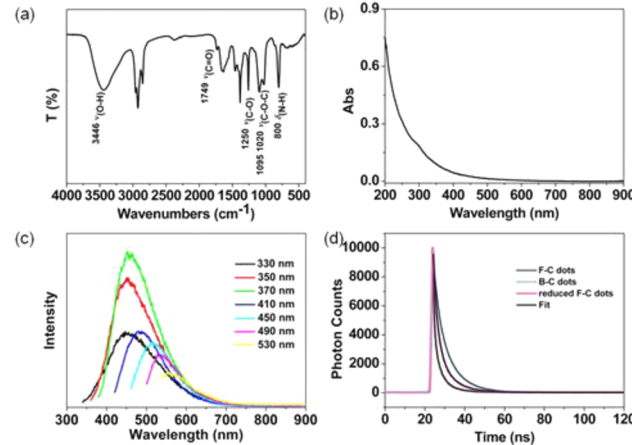


**Figure 4.** (a) FT-IR spectrum, (b) UV-visible absorption spectrum, and (c) fluorescence spectra of NaBH<sub>4</sub>-reduced F-C dots; (d) Fluorescence decay profiles of B-C dots, F-C dots and reduced F-C dots at 288, 400, and 366 nm excitation, respectively.

vibrations (1250, 1095, and 1020 cm<sup>-1</sup>), and N-H bending absorption (1360, 800 cm<sup>-1</sup>) increase significantly after reduction; meanwhile, the vibrational absorption of C=O at 1749 cm<sup>-1</sup> and C=N 1668 cm<sup>-1</sup> decrease greatly with only a small peak of C=O remaining, which clearly indicates most of the C=O and C=N groups are reduced.

The variation in surface functional groups results in the change in UV-vis absorption spectra. Similar to literature reports, the B-C dots show characteristic absorption at 228 nm for  $\pi \rightarrow \pi^*$  transition of aromatic sp<sup>2</sup> domains, with a tail extending into the visible range.<sup>3,27,28</sup> In addition, another shoulder peak at 282 nm, which can be ascribed to n  $\rightarrow \pi^*$  of C=O, is also observed (Figure 1b).<sup>27</sup> For F-C dots, the shoulder peaks located at 300 and 421 nm are observed (Figure 1b). These two shoulder peaks almost disappear with only a small remaining peak before 300 nm after the reduction with NaBH<sub>4</sub> (Figure 4b). Combining the structural characteristic and spectral changes of the B-C dots and F-C dots, the absorption peaks at 421 nm in F-C dots are ascribed to electron transition of n  $\rightarrow \pi^*$  for C=N. n  $\rightarrow \pi^*$  transition features a blue shift of absorption peak with the increase of dielectric constant of the solvent. Here, as the solvent changes from CH<sub>2</sub>Cl<sub>2</sub> to H<sub>2</sub>O, a blue shift of absorption peak was observed; this result supports our assignment (Figure S10 in the SI). The absorption peaks at 300 nm in F-C dots is assigned to the n  $\rightarrow \pi^*$  transition for C=O. The red shifts of n  $\rightarrow \pi^*$  transition absorption for C=O from 282 nm (B-C dots) to 300 nm (F-C dots) may be from the effects of C=N groups on the energy levels of C dots.

Meanwhile, the emission intensities at the green and red region decrease greatly, and the emission positions blue shift after reduction with NaBH<sub>4</sub> (Figure 4c). Fluorescence lifetime

measurements of these C dots are also carried out. The decay curve of B-C dots, as shown in Figure 4d, can be fitted by a double-exponential function with lifetimes of 2.41 ns (14.51%) and 8.03 ns (85.49%) at 288 nm excitation, with an intensity-weighted average time of 7.76 ns. For the F-C dots, the decay curve exhibits a three-exponential decay with the lifetime of 0.45 ns (29.71%), 2.83 ns (42.73%), and 8.13 ns (27.56%) at 400 nm excitation, with an intensity-weighted average time of 6.06 ns. As we know, diverse fluorophores or energy levels present in the samples are responsible for their multiple lifetimes. Thus, it can be deduced that new energy levels are generated in F-C dots compared with B-C dots from the lifetime data. In addition, when the C=O and C=N groups in F-C dots are reduced by NaBH<sub>4</sub>, the fluorescence decay curve of the reduced C dots can be fitted well with a double-exponential decay function with life times of 2.19 ns (19.85%) and 7.77 ns (80.15%), yielding an intensity-weighted average lifetime of 7.40 ns after removing some of the energy levels. Consequently, we can conclude that the introduction of C=O and C=N in F-C dots causes effective electron transitions at 4.1 eV (300 nm, n → π\* of C=O) and 2.9 eV (421 nm, n → π\* of C=N), and subsequently provides a new energy level into the electronic structures of F-C dots, resulting in fluorescence at longer wavelength and shortened fluorescence lifetime meanwhile.

Then the energy level diagram of the B-C dots and F-C dots are proposed as illustrated in Figure 5, and we propose that (i)

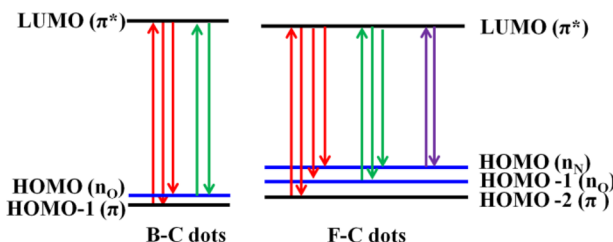


**Figure 5.** Schematic illustration for proposed energy level and electron transition diagrams of B-C dots and F-C dots.

F-C dots feature core structures similar to those of B-C dots, and their full-color emissions are mainly derived from different surface states; (ii) For the F-C dots, except for the HOMO-2 (π) energy level, two new HOMO-1 and HOMO are introduced by n<sub>C=O</sub> and n<sub>C=N</sub>. Then, electron transitions can happen from the two new HOMO-1 and HOMO to the LUMO (π\*); meanwhile, the excited electrons can be deactivated by radiative recombination, leading to fluorescence in the green and red regions. For the B-C dots, a small amount of C=O is present in its structure from IR analysis, which can only induce weak green fluorescence as their low transition probability (Figure 1c); (iii) the excited electrons generated by absorption of short wavelength light (HOMO-2(π) → LUMO(π\*)) can relax to the HOMO-2, HOMO-1, and HOMO through radiative recombination and result in the broad and asymmetric emission from the blue to the red region.

To confirm the above conclusion, C dots with different surface functional groups are prepared by varying the volume ratio of DEA to CHCl<sub>3</sub> from 1:10 to 2:1. The resulting C dots also feature full-color emission properties (Figure S11a in the SI). It is worth noting that the variation of PL intensity in the green and red regions are consistent with change of contents for C=O and C=N groups on the surface of C dots (Figure

S11b in the SI). This result further confirms that the emission in the green and red regions was derived from direct recombination of the excited electrons from the n → π\* transitions of the surface C=O and C=N groups. In addition, the emission range and peak positions for the resulted C dots with reaction time from 6 to 60 h did not change; only intensity variations were observed (Figure S12 in the SI). These phenomena are quite different from those of the C dots with colorful emission originating from different sizes or nano-domains, whose emission red-shifts gradually with larger size and longer reaction time.<sup>44</sup>

To further prove our proposal, the excitation spectra of B-C dots and F-C dots and reduced F-C dots are also investigated (Figures S13, S14, S15 in the SI). First, as shown in Figure S14 in the SI, except for the π → π\* transition from the carbon core, the green and red emissions of F-C dots have sharp excitation peaks near the emission, suggesting that electron transitions can happen from the HOMO-1 (n<sub>C=O</sub>) and HOMO (n<sub>C=N</sub>) ground states to LUMO (π\*). In addition, these phenomena are quite different from carbon dots with multicolor emission originating from different sizes, which have broad featureless excitation spectra at different emission wavelengths.<sup>25</sup> Second, the emissions at the green and red region surely have several nearly fixed excitation peaks at shorter wavelengths (370, 536, 636 nm), which agrees with the deduction that the excited electrons from LUMO (π\*) can relax to the HOMO-2, HOMO-1, and HOMO ground states by radiative relaxation. After reduction of the surface groups, the excitation peaks at 536 nm and 636 nm almost disappear by eliminating most of the ground state from C=O and C=N.

**Formation Mechanism of C Dots.** The mechanism investigation on the formation of C dots from the bottom-up method is very challenging and usually not employed, due to the difficulties in tracking and characterizing the complicated reactions. Here, we are committed to understand the formation mechanism based on possible routes of organic reactions and the available characterizations of obtained intermediates. First, we hypothesized that CHCl<sub>3</sub> generates dichlorocarbene in the presence of DEA by an elimination reaction.<sup>45</sup> Dichlorocarbene, as an active species, undergoes an insertion reaction with N–H and C–H.<sup>46,47</sup> Then substitution of DEA with chlorine,<sup>48</sup> elimination of HCl, and the rearrangement reaction all happen simultaneously to generate cycloenes or alkenes.<sup>49,50</sup> Cycloenes or alkenes continue to react with dichlorocarbene to generate larger fused rings.<sup>51,52</sup> As the carbon condensation proceeds, the cores of C dots are formed and crystallized through heating. The above proposed reaction mechanism is supported by the following experiment results. First, diethylammonium chloride is detected from the reaction, which is confirmed by high-resolution mass spectrometry (HRMS) and <sup>1</sup>H NMR. Second, bis(N,N-diethylamino)cyclopropene, bis(N,N-diethylamino)cyclopentadiene, and tri(N,N-diethylamino)cyclopropene, with their mass peaks respectively at 183.1855, 209.2011, and 254.2583, are found in HRMS detection of the generated reaction intermediate (Figure S16 in the SI). These results evidently suggest the generation of cycloene compounds from the active intermediate of dichlorocarbene during the reaction. Then the formation of fused rings is proved by <sup>13</sup>C NMR spectra of the C dots with signals in the δ = 110–180 ppm range (Figure S17 in the SI). In comparison with C dots prepared from the top-down method, more sp<sup>3</sup> carbonates are generated in our C dots with unsaturated organic small molecules as reactant intermediates. Because the syntheses are

done under air, many reaction types with different reaction rates are possible, and multitudinous oxygen-containing and nitrogen-containing functional groups are formed on the surface as confirmed by XPS and IR analyses.

Despite the reaction complexity, the generation of the B-C dots and F-C dots follows a very simple rule. Figure S14 in the SI shows the fluorescence spectra evolution of C dots with reaction time. Within the first hour of reaction, the main product is B-C dots (Figure 1c). When the time is prolonged to 24 h, in addition to the B-C dots, the emissions of F-C dots centered at green and red regions appear simultaneously. Also, the intensity ratio of the characteristic emission of B-C dots at 407 nm to F-C dots at 556 nm decreased from 3.2 to 2.2 as the reaction time increased from 24 to 60 h, which indicates that the relative content of F-C dots in the products gradually increases with longer reaction time (Figure S18 in the SI). Thus, it suggests that the F-C dots are transformed from B-C dots, because if F-C dots and B-C dots grow separately, the intensity ratio of these two types of C dots would not change with reaction time. In addition, only the emission intensity of F-C dots increases with reaction time, while the emission peak positions with the same excitation wavelengths are almost fixed, which suggests both B-C dots and F-C dots are stable species, which are the main components of the fluorescent products.

#### Application of F-C Dots in Ratiometric pH Sensing.

The excitation-dependent full-color emission property makes our F-C dots very robust in constructing functional sensing systems with a wide range of emitters. Nanoparticle-based pH sensors, which usually incorporate at least two type of dyes, can be utilized in single excitation mode or dual excitation mode for achieving ratiometric fluorescence detection.<sup>53–58</sup> Here, the pH-sensitive dye, fluorescein isothiocyanate (FITC), the emission intensity of which increases with increased pH values, is used as a model of functional molecules to construct a ratiometric pH sensor. Different from the previously reported pH sensor using C dots as carrier,<sup>57</sup> our F-C dots are applied as an internal reference. Because the emission of the obtained F-C dots covers the whole visible spectra, there are surely two or more fluorescence intensity references for the quantification of pH value. In this case, both single excitation mode and dual excitation mode are available with this sensor. Thus, several independent results can be cross-calibrated to determine the measurement reliability in case there are measurement errors or interferences from the environment. We believe these FITC-modified F-C dots (FITC-C dots) are excellent nanosensors for pH value.

FITC-C dots are prepared in anhydrous methanol by reaction of the isothiocyanate group in FITC with amino group in F-C dots and purified by dialysis. IR spectra prove that FITC is conjugated to C dots (Figure S19 in the SI).<sup>59</sup> In addition, a fluorometric method is developed for the determination of the amount of FITC linked to F-C dots (Figure S20 in the SI). When the weight ratio of F-C dots to FITC is 100:1 during the reaction, the amount of FITC conjugated to the F-C dots per milligram is calculated to be about 0.0088 mg. Such a protocol results in the FITC-C dots with both the emissions of FITC and F-C dots; meanwhile, the resulted FITC-C dots can possess an optimized linear relationship with the pH values.

Figure 6a shows the fluorescence spectra of the FITC-C dots as a function of the pH value. A stronger emission peak at 524 nm from FITC and a hump emission at around 470 nm from the F-C dots appear together when excited at 405 nm. When

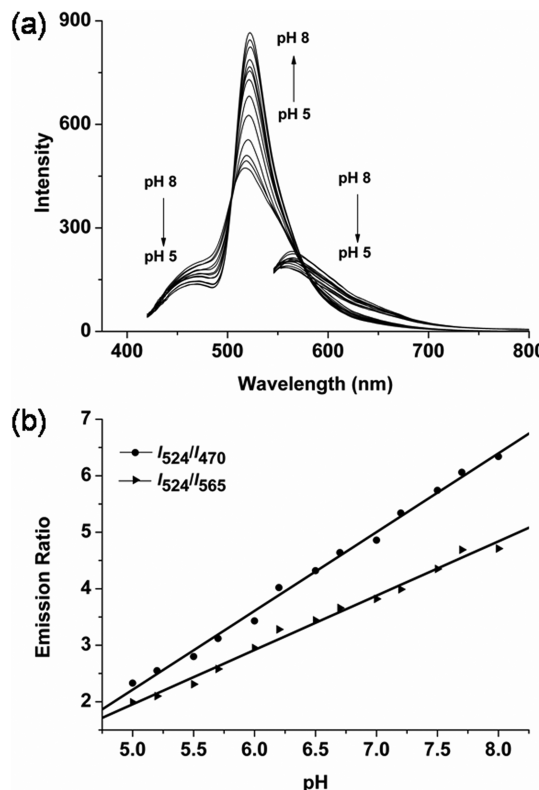


**Figure 6.** (a) Fluorescence spectra of FITC-C dots at different pHs ranging from 5 to 8. Excitation wavelengths are 405 and 543 nm; (b) Ratiometric pH calibration plots of the emission ratio  $I_{524}/I_{470}$  and  $I_{524}/I_{565}$  of FITC-C dots as a function of pH.

excited at 543 nm, another emission peak around 565 nm appears. The emission peak at 524 nm increases with increasing pH, while the fluorescence values at 470 and 565 nm decrease little with pH, and these are used as references. Then, the pH value can be determined by measuring the fluorescence intensity ratio of FITC residues at 524 nm to F-C dots residues at 470 nm in single excitation mode (excited at 405 nm) and to F-C dots residues at 565 nm in dual excitation mode (excited at 405 and 543 nm) concurrently. In this way, two independent standard curves are obtained (Figure 6b). It is found that the fluorescence intensity ratios change linearly in the range from pH = 5 to pH = 8 for the FITC-C dots. In addition, this system with two references can give two measurement results in comparison to sensors with one reference, thereby giving even more reliable and accurate measurements. This is a very exciting result because many chemical processes and major illnesses including cancers are closely related to pH variation. Then the newly designed FITC-C dots pH sensor with high accuracy will find a broad range of application in monitoring chemical reactions and diagnosis of cancers and many major illnesses *in vivo*.

MTT (3-(4,5-Dimethylthiazol-2-yl)-2,5-diphenyltetrazolium bromide) assays of cell viability studies show greater than 80% cell viability rate for F-C dots with concentrations up to 0.2 mg/mL for 24 h. In comparison with semiconductor quantum dots, a 50% loss for porcine renal proximal cells after exposure to PEGylated CdSe/ZnS QDs at 10 nM for 24 h suggests the low cytotoxicity of the as-prepared C dots (Figure S21 in the SI).<sup>13,14</sup> Then our FITC-C dots pH sensor can be applied for intracellular pH detection.

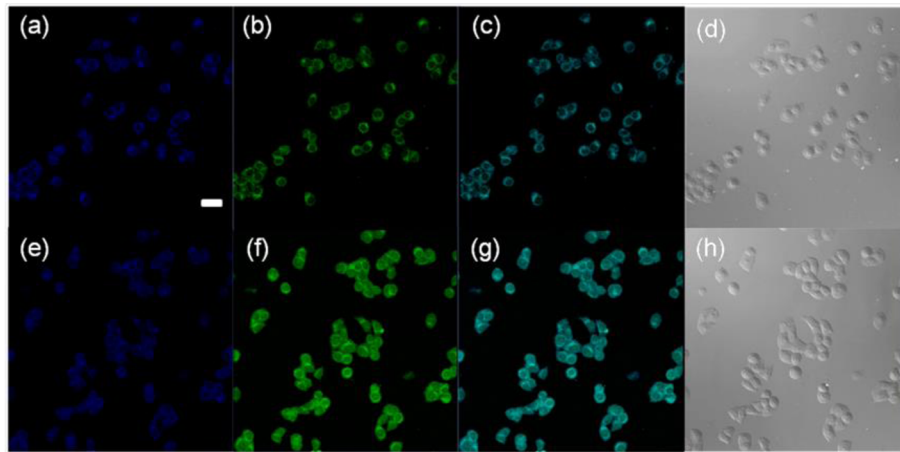


**Figure 7.** Fluorescent images of HeLa cells labeled by F-C dots (the first row) and FITC-C dots (the second row) respectively. The images of (a) and (e) are collected in the ranges of 440–480 nm at  $\lambda_{\text{ex}} = 405$  nm (channel a); The images of (b) and (f) are collected in the ranges of 500–540 nm at  $\lambda_{\text{ex}} = 405$  nm (channel b); The images of (c) are the overlay of (a) and (b), (g) is the overlay of (e) and (f). Their corresponding bright-field images are shown in (d) and (h), respectively. Scale bar = 20  $\mu\text{m}$ .

Intracellular pH plays a pivotal role in cellular processes, and changes in pH can have a drastic effect on biomolecular structure and enzyme activity.<sup>60</sup> However, the brightness and cytotoxicity of the reported sensors still await further improvement for *in vivo* biological applications. Because of the low toxicity of our FITC-C dots, they are introduced into HeLa cells via endocytosis for measuring intracellular pH. Here, by incubating cells with FITC-C dots at 4 °C, little uptake of the FITC-C dots was observed (Figure S22 in the SI), suggesting the endocytosis mechanism for the cellular uptake of FITC-C dots in our experiments performed at 37 °C.<sup>61</sup> Bare F-C dots without FITC served as the negative control (Figure 7a–d). Figure 7e–h show the confocal fluorescence microscopy images of HeLa cells after the endocytosis of FITC-C dots. From the high-resolution confocal images (Figure S23 in the SI), we can know the FITC-C dots were not evenly distributed throughout the whole cell. By integrating the spectral region from 440 to 480 nm (channel a, Figure 7a and 7e) and 500 to 540 nm (channel b, Figure 7b and 7f) at  $\lambda_{\text{ex}} = 405$  nm for F-C dots and FITC-C dots, the intracellular pH is determined by comparing the average fluorescence intensity ratio between channel b and channel a to the pH standard curves. The fluorescent signals in channels a and b were quantified based on at least 50 individual cells from the confocal images,<sup>62</sup> and the intensity ratio of  $I_{\text{channel b}}/I_{\text{channel a}}$  is calculated to be  $2.39 \pm 0.18$ , which corresponded to  $\text{pH} = 5.1 \pm 0.4$  in the pH standard curve. This value is in good accordance with the reported value.<sup>63</sup> From the above measured pH value, we can deduce that the FITC-C dots are mainly located in lysosomes. In order to verify this deduction, a colocalization experiment was performed by costaining HeLa cells with FITC-C dots and Lysotracker@Red DND-99. As shown in Figure S24 in the SI, the intensity profiles along the line of interest across HeLa cells share similar changes with Pearson's coefficient of 0.68, indicating lysosomes are the main site of FITC-C dots accumulation.<sup>64</sup> Meanwhile, the influences of intracellular species, such as  $\text{Na}^+$ ,  $\text{K}^+$ , glucose, bovine serum albumin, etc. on the measurement of pH value are investigated. The obtained results show that these species have almost no effect on the quantification of pH values (Figure S25 in the SI). Although the FITC-C dots have been developed as a double reference for the ratiometric pH sensor using the fluorescence

spectrophotometer and it is useful to determine the pH values of special systems where a pH meter is invalid, it is hard to realize the cross-calibration with confocal fluorescence microscopy, because it is difficult to regulate the two excitation wavelengths to the same intensity as in the fluorescence spectrophotometer. There are reports that the ratiometric pH calibration plots can be obtained *in situ* with confocal fluorescence microscopy,<sup>57</sup> and then the cross-calibration of the two references from our FITC-C dots pH sensor can be achieved. However, at the present stage, we do not have the facility to do such experiments.

## ■ CONCLUSIONS

In conclusion, excitation-independent blue fluorescent C dots and excitation-dependent full-color fluorescent C dots have been prepared by a highly reproducible new route. The C dots have fair quantum yield and good compatibility and stability. By a great amount of detailed work, it is found that the surface functional groups of  $\text{C}=\text{O}$  and  $\text{C}=\text{N}$  have efficiently introduced new energy levels for electron transitions and resulted in the continuously adjustable excitation-dependent full-color emissions within a single C dot. Taking advantage of the full-color emission and low toxicity, a ratiometric pH sensor using two emission wavelengths of the F-C dots as independent references has been constructed to improve the measurement reliability and accuracy and has been applied to detect the intracellular pH values accurately. Thus, our work makes significant progress toward engineering the emission properties of C dots and demonstrates the great potentials of C dots as unique emitters. What's more, the excitation-dependent full-color emission properties of C dots will open the door to a host of new applications, such as a multistates logic gate, by tuning the emission states with a combination of different excitation wavelengths, which is underway in our lab.

## ■ ASSOCIATED CONTENT

### S Supporting Information

Experimental details and supporting figures. This material is available free of charge via the Internet at <http://pubs.acs.org>.

## AUTHOR INFORMATION

### Corresponding Authors

\*E-mail: liminjie@jlu.edu.cn (M.L.).

\*E-mail: seanzhang@jlu.edu.cn (S.X.-A.Z.). Fax: 0431-85153812.

### Notes

The authors declare no competing financial interest.

## ACKNOWLEDGMENTS

This work was supported by the National Natural Science Foundation of China (51001020, 21072025). We acknowledge Zhinan Guo for Raman analysis, engineer Yan Zhang in Core Facilities for Life Science in Jilin University for confocal fluorescence microscopy test, and Professor Changfeng Wu for helpful discussion.

## REFERENCES

- (1) Baker, S. N.; Baker, G. A. *Angew. Chem., Int. Ed.* **2010**, *49*, 6726.
- (2) Li, H.; Kang, Z.; Liu, Y.; Lee, S.-T. *J. Mater. Chem.* **2012**, *22*, 24230.
- (3) Sun, Y. P.; Zhou, B.; Lin, Y.; Wang, W.; Fernando, K. A. S.; Pathak, P.; Meziani, M. J.; Harruff, B. A.; Wang, X.; Wang, H. *J. Am. Chem. Soc.* **2006**, *128*, 7756.
- (4) Liu, R.; Wu, D.; Liu, S.; Koynov, K.; Knoll, W.; Li, Q. *Angew. Chem., Int. Ed.* **2009**, *48*, 4598.
- (5) Bourlinos, A. B.; Stassinopoulos, A.; Anglos, D.; Zboril, R.; Karakassis, M.; Giannelis, E. P. *Small* **2008**, *4*, 455.
- (6) Liu, H.; Ye, T.; Mao, C. *Angew. Chem., Int. Ed.* **2007**, *46*, 6473.
- (7) Liu, S.; Tian, J.; Wang, L.; Luo, Y.; Zhai, J.; Sun, X. *J. Mater. Chem.* **2011**, *21*, 11726.
- (8) Li, H.; He, X.; Kang, Z.; Huang, H.; Liu, Y.; Liu, J.; Lian, S.; Tsang, C. H. A.; Yang, X.; Lee, S. T. *Angew. Chem., Int. Ed.* **2010**, *49*, 4430.
- (9) Xu, X.; Ray, R.; Gu, Y.; Ploehn, H. J.; Gearheart, L.; Raker, K.; Scrivens, W. A. *J. Am. Chem. Soc.* **2004**, *126*, 12736.
- (10) Eda, G.; Lin, Y. Y.; Mattevi, C.; Yamaguchi, H.; Chen, H. A.; Chen, I.; Chen, C. W.; Chhowalla, M. *Adv. Mater.* **2010**, *22*, 505.
- (11) Zhu, S.; Meng, Q.; Wang, L.; Zhang, J.; Song, Y.; Jin, H.; Zhang, K.; Sun, H.; Wang, H.; Yang, B. *Angew. Chem., Int. Ed.* **2013**, *52*, 3953.
- (12) Cao, L.; Wang, X.; Meziani, M. J.; Lu, F.; Wang, H.; Luo, P. G.; Lin, Y.; Harruff, B. A.; Veca, L. M.; Murray, D.; Xie, S.-Y.; Sun, Y.-P. *J. Am. Chem. Soc.* **2007**, *129*, 11318.
- (13) Yang, S.-T.; Cao, L.; Luo, P. G.; Lu, F.; Wang, X.; Wang, H.; Meziani, M. J.; Liu, Y.; Qi, G.; Sun, Y.-P. *J. Am. Chem. Soc.* **2009**, *131*, 11308.
- (14) Yang, S.-T.; Wang, X.; Wang, H.; Lu, F.; Luo, P. G.; Cao, L.; Meziani, M. J.; Liu, J.-H.; Liu, Y.; Chen, M.; Huang, Y. P.; Sun, Y.-P. *J. Phys. Chem. C* **2009**, *113*, 18110.
- (15) Wei, W.; Xu, C.; Wu, L.; Wang, J.; Ren, J.; Qu, X. *Sci. Rep.* **2014**, *4*, 3564.
- (16) Wang, J.; Wang, C. F.; Chen, S. *Angew. Chem., Int. Ed.* **2012**, *51*, 9297.
- (17) Cao, L.; Sahu, S.; Anilkumar, P.; Bunker, C. E.; Xu, J.; Fernando, K. S.; Wang, P.; Gulians, E. A.; Tackett, K. N.; Sun, Y.-P. *J. Am. Chem. Soc.* **2011**, *133*, 4754.
- (18) Zhuo, S.; Shao, M.; Lee, S.-T. *ACS Nano* **2012**, *6*, 1059.
- (19) Liu, S.; Tian, J.; Wang, L.; Zhang, Y.; Qin, X.; Luo, Y.; Asiri, A. M.; Al-Youbi, A. O.; Sun, X. *Adv. Mater.* **2012**, *24*, 2037.
- (20) Lu, W.; Qin, X.; Liu, S.; Chang, G.; Zhang, Y.; Luo, Y.; Asiri, A. M.; Al-Youbi, A. O.; Sun, X. *Anal. Chem.* **2012**, *84*, 5351.
- (21) Shi, W.; Wang, Q.; Long, Y.; Cheng, Z.; Chen, S.; Zheng, H.; Huang, Y. *Chem. Commun.* **2011**, *47*, 6695.
- (22) Zhou, L.; Lin, Y.; Huang, Z.; Ren, J.; Qu, X. *Chem. Commun.* **2012**, *48*, 1147.
- (23) Dong, Y.; Pang, H.; Yang, H. B.; Guo, C.; Shao, J.; Chi, Y.; Li, C. M.; Yu, T. *Angew. Chem., Int. Ed.* **2013**, *52*, 7800.
- (24) Long, Y. M.; Zhou, C. H.; Zhang, Z. L.; Tian, Z. Q.; Bao, L.; Lin, Y.; Pang, D. W. *J. Mater. Chem.* **2012**, *22*, 5917.
- (25) Zhang, Y.-Q.; Ma, D.-K.; Zhuang, Y.; Zhang, X.; Chen, W.; Hong, L.-L.; Yan, Q.-X.; Yu, K.; Huang, S.-M. *J. Mater. Chem.* **2012**, *22*, 16714.
- (26) Zhu, S.; Zhang, J.; Tang, S.; Qiao, C.; Wang, L.; Wang, H.; Liu, X.; Li, B.; Li, Y.; Yu, W. *Adv. Funct. Mater.* **2012**, *22*, 4732.
- (27) Tang, L.; Ji, R.; Cao, X.; Lin, J.; Jiang, H.; Li, X.; Teng, K. S.; Luk, C. M.; Zeng, S.; Hao, J.; Lau, S. P. *ACS Nano* **2012**, *6*, 5102.
- (28) Tang, L.-B.; Ji, R.-B.; Li, X.-M.; Teng, K.-S.; Lau, S.-P. *J. Mater. Chem. C* **2013**, *1*, 4908.
- (29) Guo, X.; Wang, C.-F.; Yu, Z.-Y.; Chen, L.; Chen, S. *Chem. Commun.* **2012**, *48*, 2692.
- (30) Zhou, J.; Booker, C.; Li, R.; Zhou, X.; Sham, T. K.; Sun, X.; Ding, Z. *J. Am. Chem. Soc.* **2007**, *129*, 744.
- (31) Li, Y.; Zhao, Y.; Cheng, H.; Hu, Y.; Shi, G.; Dai, L.; Qu, L. *J. Am. Chem. Soc.* **2011**, *134*, 15.
- (32) Wolkin, M. V.; Jorne, J.; Fauchet, P. M. *Phys. Rev. Lett.* **1999**, *82*, 197.
- (33) Hsu, P. C.; Chang, H. T. *Chem. Commun.* **2012**, *48*, 3984.
- (34) Mei, Q.; Zhang, K.; Guan, G.; Liu, B.; Wang, S.; Zhang, Z. *Chem. Commun.* **2010**, *46*, 7319.
- (35) Ray, S. C.; Saha, A.; Jana, N. R.; Sarkar, R. *J. Phys. Chem. C* **2009**, *113*, 18546.
- (36) Kim, E.; Koh, M.; Ryu, J.; Park, S. B. *J. Am. Chem. Soc.* **2008**, *130*, 12206.
- (37) Higashiguchi, K.; Matsuda, K.; Tanifugi, N.; Irie, M. *J. Am. Chem. Soc.* **2005**, *127*, 8922.
- (38) Lee, J.; Sundar, V. C.; Heine, J. R.; Bawendi, M. G.; Jensen, K. F. *Adv. Mater.* **2000**, *12*, 1102.
- (39) Chen, P.-C.; Chen, Y.-N.; Hsu, P.-C.; Shih, C.-C.; Chang, H.-T. *Chem. Commun.* **2013**, *49*, 1639.
- (40) Yu, P.; Wen, X.; Toh, Y.-R.; Tang, J. *J. Phys. Chem. C* **2012**, *116*, 25552.
- (41) Peng, J.; Gao, W.; Gupta, B. K.; Liu, Z.; Aburto, R. R.; Ge, L.; Song, L.; Hayashi, T.; Zhu, J.-J.; Ajayan, P. M. *Nano Lett.* **2012**, *12*, 844.
- (42) Zheng, H.; Wang, Q.; Long, Y.; Zhang, H.; Huang, X.; Zhu, R. *Chem. Commun.* **2011**, *47*, 10650.
- (43) Cimarelli, C.; Palmieri, G. *Tetrahedron: Asymmetry* **2000**, *11*, 2555.
- (44) Wen, X.; Yu, P.; Toh, Y.-R.; Lee, Y.-C.; Hsu, A.-C.; Tang, J. *Appl. Phys. Lett.* **2012**, *101*, 163107.
- (45) Mihara, M.; Ishino, Y.; Minakata, S.; Komatsu, M. *J. Org. Chem.* **2005**, *70*, 5320.
- (46) Seyferth, D.; Washburne, S. S.; Attridge, C. J.; Yamamoto, K. J. *Am. Chem. Soc.* **1970**, *92*, 4405.
- (47) Fields, E. K. *J. Am. Chem. Soc.* **1962**, *84*, 1744.
- (48) Clark, G. R.; Surman, P. W.; Taylor, M. J. *J. Chem. Soc., Faraday Trans.* **1995**, *91*, 1523.
- (49) Keating, A. E.; Merrigan, S. R.; Singleton, D. A.; Houk, K. J. *Am. Chem. Soc.* **1999**, *121*, 3933.
- (50) Bartmann, E.; Mengel, T. *Angew. Chem., Int. Ed.* **1984**, *23*, 225.
- (51) Smith, K. A.; Streitwieser, A., Jr. *J. Org. Chem.* **1983**, *48*, 2629.
- (52) Zhu, M.; Wang, J.; Holloway, B. C.; Outlaw, R.; Zhao, X.; Hou, K.; Shutthanandan, V.; Manos, D. M. *Carbon* **2007**, *45*, 2229.
- (53) Benjamin, R. V.; Sun, H.; Henriksen, J. R.; Christensen, N. M.; Almdal, K.; Andresen, T. L. *ACS Nano* **2011**, *5*, 5864.
- (54) Hornig, S.; Biskup, C.; Gräfe, A.; Wotschadlo, J.; Liebert, T.; Mohr, G. J.; Heinze, T. *Soft Matter* **2008**, *4*, 1169.
- (55) Sun, H.; Scharff-Poulsen, A. M.; Gu, H.; Almdal, K. *Chem. Mater.* **2006**, *18*, 3381.
- (56) Chan, Y.-H.; Wu, C.; Ye, F.; Jin, Y.; Smith, P. B.; Chiu, D. T. *Anal. Chem.* **2011**, *83*, 1448.
- (57) Shi, W.; Li, X.; Ma, H. *Angew. Chem., Int. Ed.* **2012**, *51*, 6432.
- (58) Jin, T.; Sasaki, A.; Kinjo, M.; Miyazaki, J. *Chem. Commun.* **2010**, *46*, 2408.
- (59) McKinney, R. M.; Spillane, J. T.; Pearce, G. W. *Anal. Biochem.* **1966**, *14*, 421.

- (60) Han, J.; Burgess, K. *Chem. Rev.* **2009**, *110*, 2709.  
(61) Wong, N.; Kam, S.; Dai, H. *J. Am. Chem. Soc.* **2005**, *127*, 6023.  
(62) Vukojević, V.; Heidkamp, M.; Ming, Y.; Johansson, B.; Terenius, L.; Rigler, R. *Proc. Natl. Acad. Sci. U.S.A.* **2008**, *105*, 18176.  
(63) Bayer, N.; Schober, D.; Prchla, E.; Murphy, R. F.; Blaas, D.; Fuchs, R. *J. Virol.* **1998**, *72*, 9645.  
(64) Yu, H.; Xiao, Y.; Jin, L. *J. Am. Chem. Soc.* **2012**, *134*, 17486.